Cellulose (2024) 31:7385–7403
https://doi.org/10.1007/s10570-024-06078-2

ORIGINAL RESEARCH

Enhancement of cellulose nanofibril (CNF) film barrier properties by nanofibril alignment

Nabanita Das · Islam Hafez · Douglas W. Bousfield · Mehdi Tajvidi

Received: 12 April 2024 / Accepted: 19 July 2024 / Published online: 24 July 2024

Abstract This study is centered on improving the mechanical and barrier characteristics of cellulose nanofibril films for food packaging applications. The goal was to induce fibril orientation, which was achieved by fabricating CNF films via an auto-dynamic sheet former (ADSF) at varying wire speeds, and varying CNF suspension solid contents. The wet-laid films were then dried using restrained (Z_Z shrinkage) and non-restrained (XY_Z) methods. Z_Z films demonstrated higher strength compared to XY_Z films at wire speeds of 1000 m/min and 1100 m/min. Films produced at 1100 m/min demonstrated the best oxygen barrier properties, irrespective of the drying technique employed. For 1100 m/min 0.1 wt.% films, the oxygen permeability values were decreased by 51.7% for the Z_Z shrinkage drying method and 40.3% for the XY_Z shrinkage drying method when compared to 900 m/min 0.1 wt.% films. The orientation of the film was assessed using polarized light microscopy (PLM) and wide-angle X-ray scattering (WAXS). However, these methods seemed to be limited to specific instances, as only a small area of the film could be imaged which did not provide a comprehensive indication of the overall alignment of the film, likely due to averaging of film's response to these techniques caused by their multi-layer structure. Future research could delve deeper into producing oxygen barrier packaging materials using similar formulations in a paper-forming machine. Additionally, a potential future study could explore depositing an aligned CNF layer directly onto the paper substrate to form sustainable food containers made of paper.

Keywords Cellulose nanofibrils · Orientation · Mechanical properties · Barrier properties · Dynamic sheet former

Supplementary Information The online version contains supplementary material available at https://doi.org/10.1007/s10570-024-06078-2.

N. Das · M. Tajvidi (✉)
School of Forest Resources, University of Maine, 5755 Nutting Hall, Orono, ME 04469, USA
e-mail: mehdi.tajvidi@maine.edu

N. Das
e-mail: nabanita.das@maine.edu

I. Hafez
Wood Science and Engineering, Oregon State University, 108 Richardson Hall, Corvallis, OR 97331, USA
e-mail: Islam.Hafez@oregonstate.edu

D. W. Bousfield
Chemical and Biomedical Engineering, University of Maine, 117 Jenness Hall, Orono, ME 04469, USA
e-mail: bousfld@maine.edu

M. Tajvidi
Advanced Structures and Composites Center, University of Maine, 35 Flagstaff Road, Orono, ME 04469, USA

Introduction

Plastic materials like polyethylene (PE), polystyrene (PS), and polypropylene (PP) are widely used for food packaging across the globe (Ncube et al. 2020). The plastic food packaging industry has seen a surge in demand during the COVID-19 pandemic, especially for single-use containers. These materials are popular because they are affordable, flexible, and resistant to chemical, mechanical, and microbial damage. The higher oxygen barrier of these plastic food packaging materials helps to extend the shelf life of food, preserve its color, odor, and flavor during storage and transportation, reduce the risk of bacterial and fungal attacks, and keep the food fresh (Zabihzadeh Khajavi et al. 2020).

A considerable amount of plastic waste generated globally is not disposed of properly, and a significant portion of it ends up in oceans or landfills (Tucki et al. 2022). There is a risk of harmful chemicals such as carcinogens leaching out from plastic wraps and food containers into the food, posing a threat to human health especially when hot food is served (Geueke et al. 2023).

To meet the demands of contemporary society for efficient packaging materials, while simultaneously being sustainable and renewable, we need to explore new approaches for improving the potential of cellulose-based materials. Cellulose is the most abundant polymer on earth. β-1,4D-glucopyranose ($C_6H_{12}O_6$) units form cellobiose, and cellulose is composed of the repeating unit of cellobiose. Much of our packaging system currently uses cellulose fibers such as boxes and paper wraps, but often these paper-based solutions do not have the required barrier properties to keep food fresh.

Cellulose nanomaterials have been shown to give barrier properties such as oxygen and oil/grease resistance (Aulin et al. 2010). The main two types of cellulose nanomaterials are cellulose nanofibrils (CNFs) and cellulose nanocrystals (CNCs). CNCs have a rod-like structure, mainly produced by acid hydrolysis, and the length and width of CNCs are usually 100–500 nm and 3–50 nm, respectively (Dufresne 2017). On the other hand, CNFs have both amorphous and crystalline regions and are produced by high shear forces using a homogenizer or a refiner, among others. CNFs have a length of 500–2000 nm and a width of 20–50 nm. CNFs have a higher aspect ratio (length-to-width ratio) and are more flexible than CNCs (Xu et al. 2013).

The light weight and good mechanical properties make CNFs a potential choice as a food packaging material (Mörseburg and Chinga-Carrasco 2009). According to Fujisawa et al. 2016, the mechanical strength of a CNF film can be enhanced by the orientation of its crystallites or nanofibrils. Various techniques are available to orient CNF films, including moistened film stretching induced by mechanical force (Gindl-Altmutter et al. 2012), stretching of wet CNF film (Sehaqui et al. 2012), and the auto-dynamic sheet former (ADSF) approach (Syverud and Stenius 2009).

The moistened film stretching orientation technique involves cutting strips from the dry film to be stretched by mechanical force. These strips are then attached to pieces of wood on both ends, moistened with water, and stretched using the grips of a universal testing machine. Once stretched, the strips were dried with hot air. While this method was successful in increasing the mechanical properties of the film, it was necessary to regenerate or modify the CNF film surface prior to applying the orientation method. It should be noted that this method cannot induce orientation in the native and untreated CNF film as they are more prone to strain failure before reaching to preferred orientation threshold (Gindl-Altmutter et al. 2012; Peng et al. 2015).

To achieve an oriented CNF film through wet stretching, the wet film was sliced into strips and secured to an Instron machine's clamps. Force was then applied to partially stretch the strip. Upon completion of the pulling process, the strips were removed in a stretched conformation and dried under stretching conditions (Sehaqui et al. 2012). While this method can produce mechanically sound CNF films, it is time-consuming and requires further research to achieve industrial-scale oriented CNF films (Gindl and Keckes 2007).

Films with oriented CNFs were also produced using an auto-dynamic sheet former (ADSF), with careful consideration given to the desired grammage and density. The ADSF is a machine that can produce fiber mats by injecting aqueous fiber suspension through a nozzle onto the inside of a rotating, perforated drum. As the drum spins, the fibers align in the direction of rotation (Sunny et al. 2021) and they are dewatered. The wet oriented sheet is pressed using

a blotting paper to remove any excess water before being dried (Petroudy et al. 2017). By adjusting the nozzle, the fiber orientation within a film produced by the ADSF can be enhanced, resulting in notable changes in the film's mechanical properties (Sunny et al. 2021).

The studies referenced above aimed at orienting fibrils in the structure of a CNF film with an ultimate goal of improving its mechanical properties. Given the high mechanical anisotropy of cellulose chains (Moon et al. 2011), it is expected that such an orientation may improve the mechanical properties in the direction of the orientation. In general, amorphous regions of polymers do not exhibit significant resistance to the diffusion of small gas molecules, whereas the more tightly packed crystalline regions can indeed impede the path of such molecules (Fukuya et al. 2014). For cellulose nanocrystals, it has been shown that an improved orientation also leads to better oxygen barrier properties (Chowdhury et al. 2018). However, it remains unclear from existing literature whether a similar effect can be achieved with oriented CNFs.

The tight and layered structure of CNF films resulting from the coalescence of amorphous and crystalline regions in the cellulose assemblies, elongates the diffusion path of oxygen molecules through the thickness of the film leading to a strong barrier for oxygen (Nair et al. 2014). CNF films are known to exhibit superior oxygen barrier properties in the dry state at room temperature (RH < 50% and 25 °C). However, the oxygen penetration rate increases as relative humidity increases from 50 to 80% (Wang et al. 2020). This is because higher relative humidity can plasticize the CNF based packaging material and increase the free volume through which oxygen can permeate (Bharadwaj 2002; Dlubek et al. 2002; Muramatsu et al. 2003). The oxygen barrier properties of the CNF films can also vary depending on the drying method. A study done by Hasan et al. 2021, showed that the oxygen permeance through CNF films was lower when the films were dried using a hot press compared to casting and oven drying methods. However, the relationship between the gas barrier properties of the native CNF film and the fiber orientation in the film requires further investigations.

The goal of this research was to develop an understanding of the relationship between the orientation of CNF films and their oxygen permeability. To this end, an auto-dynamic sheet former was used to prepare oriented CNF films at various conditions, which were then tested for their barrier and mechanical properties. In addition, two drying methods were tested, and the degree of orientation was quantified and compared with randomly oriented CNF films.

Experimental

Materials

The University of Maine's Process Development Center (PDC) provided a 3 wt.% suspension of CNFs at 90% fines, derived from northern bleached softwood kraft pulp through mechanical fibrillation. Fine content refers to the percentage of fibers in a suspension that are smaller than 200 µm in length, with a 90% fine content indicating that on average, 90% of the fibers are smaller than 200 µm (Amini et al. 2020). The fine content was determined by analyzing an image of the CNF suspension with a Compact Fiber analyzer (MorFi, TechPap Inc, Techpap SAS, Gières, France).

More information regarding the production process and CNF characteristics can be found in previously published work (Ghasemi et al. 2017; Johnson et al. 2016; Nazari et al. 2016; Tajvidi et al. 2016).

Methods

Preparation of films

In this study, CNF films of target basis weight of 60 g/m^2 were prepared using two different methods. These methods are vacuum filtration, which was used to prepare control (un-oriented) samples, and auto-dynamic sheet former (CanPa® Instruments, Quebec, Canada) used to develop oriented CNF films.

Vacuum filtration method

To utilize the vacuum filtration method for film production, the CNF slurry was diluted to 0.3 wt.% with distilled water. Following this, the suspensions underwent a two-minute sonication process using a Branson 450 Sonifier (Branson Ultrasonics Corporation, Danbury, CT, USA). Next, the suspensions were transferred to a planetary mixer (Thinky 310, Thinky

Corporation, Tokyo, Japan) and mixed for one minute at 2000 rpm followed by a defoaming step which was implemented at 2200 rpm for 30 s. Once the suspensions were bubble-free and homogenous, they were vacuum filtered at 381 mm Hg over two Whatman® #5 filter papers of 11 cm diameter and 2.5 µm pore size. The filtration process was halted after 7 min when the time between two consecutive drops was at least 20 s. Finally, the films were cold pressed for 3 min at 0.2 MPa by placing them between two blotting papers to remove the excess water (Fig. 1).

Auto-dynamic sheet former

Using an auto-dynamic sheet former (ADSF), oriented CNF films were produced with controlled fiber orientation, like commercial paper machines. The process involved introducing CNF suspensions of varying solid contents (0.1 wt.%, 0.2 wt.%, and 0.3 wt.%) into a stock tank before running the machine. The instrument comprises a centrifuge drum that is lined with a forming fabric (wire) on the inside. As the centrifuge starts rotating, water is added to it and a wall of water is built up until the wire is entirely submerged in water. Following this, a traversing nozzle sprays the stock against the fabric, to form a layer of fibers. In this study, four different wire speeds (900 m/min, 1000 m/min, 1100 m/min, and 1200 m/min) were used to form the sheets. The stock suspension was deposited onto the wire mesh at a rate of 2.20 L/min using the traversing nozzle with a 3 mm inner diameter to create fibrils layer. After deposition, the dewatering process ran for 4 min at 1400 rpm to produce a wet sheet of CNFs. The sheet could not be produced using 1200 m/min and 0.1 wt.% CNF suspension as the machine could not hold the lighter suspension at the high speed.

After forming the wet sheet, it was delicately positioned onto a Flexiglass surface with two blotting papers carefully resting on top. Filter papers with 11 cm diameter were then precisely placed onto the wet sheet. Another flexible glass sheet was added to

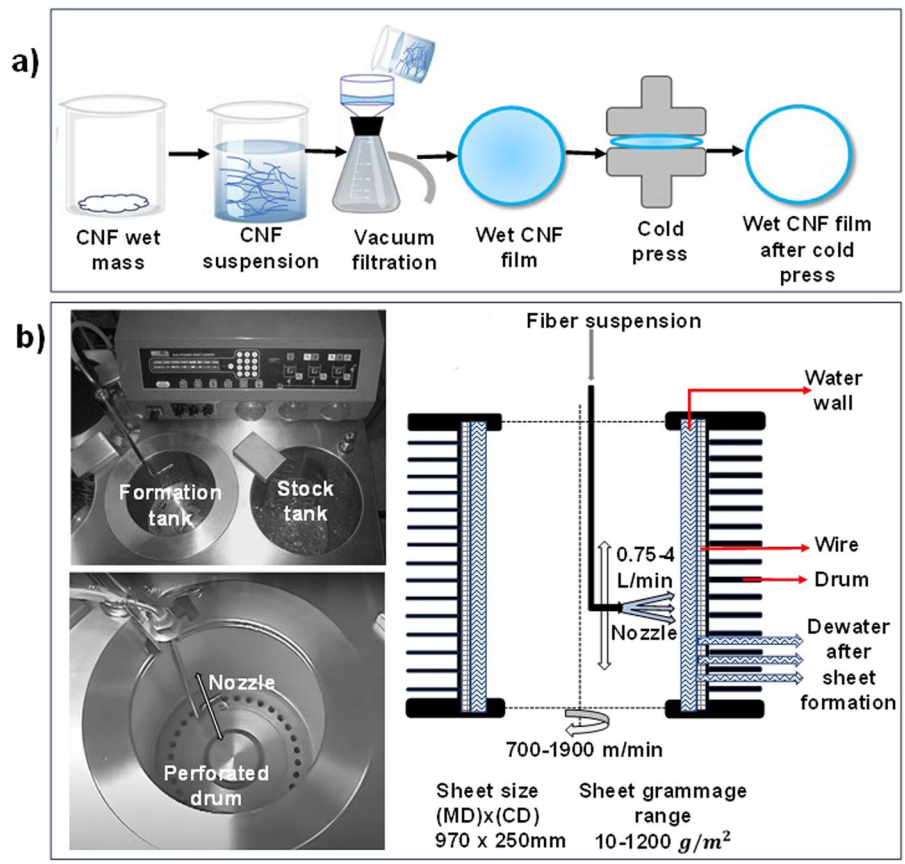

Fig. 1 Schematic diagram of vacuum filtered CNF film production (**a**) and a representation of the ADSF drum configuration (**b**)

the top of the stack before flipping it over and passing it through a two-roller sheet press with a pressure of 0.21 MPa to thoroughly eliminate any excess water. After the cold press, the top glass surface, blotting paper, and wire mesh were removed by flipping the assembly. Finally, the process was concluded by removing the films along with the filter papers from the bottom glass surface by cutting around the filter paper circles. This allowed the transfer of wet sheets onto filter paper. The orientation direction was marked on the samples, and they were placed in Ziploc bags and stored in a refrigerator at around 5 °C for further processing.

Film drying methods

Z_Z shrinkage/restrained drying

To dry the film, a pair of filter papers were positioned above and below the wet film. This stack was then placed between two stainless steel plates and heated to 150℃ for a duration of 8 min using a Carver hot-press (Carver, Inc, Wabash, IN) where the platens of the hot-press were only touching the stainless-steel plates without applying pressure. The filter papers were then removed from the film and a pressure of 1.1 MPa was applied for 4 min at the same temperature. This process was found to be effective in minimizing interfibrillar gaps and increasing the density (Hasan et al. 2021) of the film. It is worth noting that when the Z_Z shrinkage method was utilized for drying, the film only experienced shrinkage in the vertical direction and the restraint from the filter paper prevented in-plane shrinkage.

XY_Z shrinkage/non-restrained drying

To achieve XY_Z shrinkage drying, the wet film's filter paper was removed, and the film was placed on the surface of a stainless-steel plate. To prevent any pressure impact during the drying process, an aluminum spacer was used between the steel plates. The film was then hot-pressed at 150℃ for 8 min, without any pressure applied. Once dried, the film was pressed again between the steel plates for 4 min at 150℃, using the same pressure as Z_Z shrinkage drying method. The XY_Z shrinkage drying technique resulted in the film's shrinkage in both the vertical and radial directions (Fig. 2).

Characterization

Mechanical properties

Prior to testing, the specimens were conditioned in a controlled humidity chamber at 50% relative humidity and a temperature of 23 ± 2℃ for 24 h. To determine how the alignment of CNF films affects their

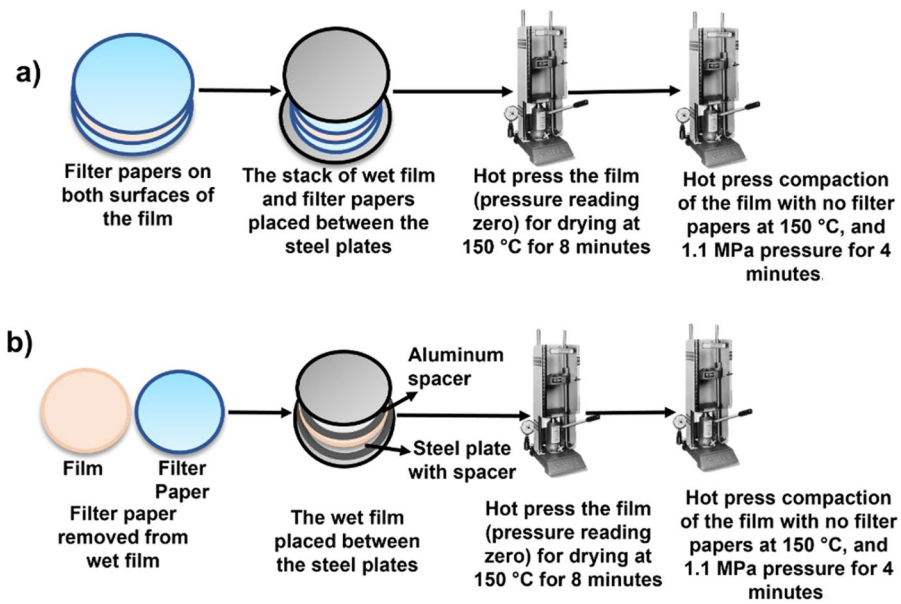

Fig. 2 Schematic diagram of **a** Z_Z shrinkage drying, **b** XY_Z shrinkage drying

mechanical strength, tensile testing was conducted in the machine and cross directions. In this context, the machine direction is the expected orientation direction parallel to the direction of the ADSF's drum rotation whereas the cross direction is the direction perpendicular to the motion direction. A universal testing machine (Model 5942, INSTRON Instruments, MA, USA) with a 500 N load cell was used to determine tensile modulus (E), tensile strength, and tensile strain. Seven strips measuring 50 mm in length and 10 mm in width were taken from both directions of the films. During testing, the crosshead motion speed was set to 2 mm/min and the actual gauge length was 20 mm. Tensile strength and modulus results were normalized by the density of the specimens. The density was determined by measuring the dimensions and mass of the samples using a Vernier caliper and an analytical balance, respectively.

Oxygen transmission rate

The oxygen transmission rate (OTR) through the films was determined using a Mocon Ox-tran 2/22 analyzer (Mocon, MN, USA), following the ASTM D3985-05 (ASTM D3985-05, 2010) protocol with a test area of 5.64 cm^2. Prior to testing, samples were conditioned for 6 h at 80% RH and 23℃ inside the machine. The sensor was cleaned through a "re-zero" process with 98% nitrogen and 2% hydrogen gas before the machine recorded the OTR value of the film using pure oxygen gas for 15 min. The test was terminated if the difference between the last measurement and the fifth measurement prior was less than 1%. If the difference exceeded expectations, the machine continued the testing cycle with another "re-zero" process after two tests. To account for variation in film thickness, OTR values were normalized, and oxygen permeability (OP) values were determined.

Birefringence orientation index (BOI)

Imaging was conducted using an AmScope polarized light microscope equipped with an AmScope HY-2307 digital camera (Model ME50TA, CA, USA). Samples were positioned on a rotating stage with a light source and marked with angles for precise placement. A red filter was utilized as the retardation filter and samples were imaged between cross polarizers, when oriented in the machine direction and placed parallel to 0° angle. Images were captured at 0°, -45°, and + 45° angles by rotating the sample which indicates that the sample was rotated clockwise (+ 45°) and counterclockwise (-45°) between cross polarizers. Cellulose nanofibrils exhibit birefringence colors, switching from blue to yellow between -45° and + 45° under the polarized light microscope, with the intensity change of the blue color indicating a shift in fiber alignment within CNF films (Ghasemi et al. 2020). The Birefringence Orientation Index (BOI) of the films was calculated using polarized light microscopy images with ImageJ software (Version 1.44, NIH, Maryland, USA), following a similar method for image analysis and noise removal to produce histogram of the BOI values as indicated in (Ghasemi et al. 2020). The BOI values were determined to represent the extent of alignment in a film, estimated from the images of intensity changes in the blue channel between angles using Eq. 1.

$$\mathrm{BOI} = \frac{b_{-45^\circ} - b_{+45^\circ}}{b_{-45^\circ} + b_{+45^\circ}} \quad (1)$$

where, b_{-45} and b_{+45} are the digital numbers (DN) of blue channel for every pixel (8 bit = 0–255) of the RGB images at their respective angles. BOI values range from − 1 to + 1. The + 1 indicates the maximum and − 1 indicates the minimum alignment in parallel to the machine directions, respectively whereas zero BOI value indicates the random orientation of fibers in the films. To obtain a clearer understanding of the orientation of films, three samples of the same production-conditions films underwent analysis using polarized light microscopy for BOI calculation. The median BOI values were calculated to minimize the impact of outliers. The resulting noise-free and smooth BOI images were then utilized to generate classified BOI maps using ArcGIS Pro (Version 2.7, ESRI, Redlands, CA, USA).

Wide-angle X-ray scattering (WAXS)

Wide angle X-ray scattering data was collected on an Anton Paar WAXSess instrument (Anton Paar GmbH, Graz, Austria) utilizing Cu-Ka radiation and line collimation. Data was recorded on an image plate in the range of 0.08–2.5 $Å^{-1}$. Sample to image plate distance of 26.1 cm. Samples were cut into 8 mm × 8 mm squares, then positioned into the center

of the sample holder. Scattering was measured for 30 min. The sample was then rotated to obtain the two desired orientations in respect to the beam as the system operated in line collimation. SAXSQUANT software (Anton Paar GmbH, Graz, Austria) was used for data collection and processing.

Statistical analysis

The objective of the research was to examine how different wire speeds and solid contents of CNF suspension affect the mechanical and oxygen barrier characteristics of the film. To accomplish this, a generalized linear model was used to conduct statistical analysis using IBM SPSS Statistics (IBM, Armonk, New York, USA), with the wire speeds and solid content of CNF suspension being utilized as factors in the analysis. The Tukey Honestly Significant Difference (HSD) test was used to identify any statistically significant differences between the means of different groups, at a 95% confidence interval ($p < 0.05$).

Results and discussion

Films physical properties

This study utilized the Z_Z and XY_Z shrinkage drying techniques. The Z_Z shrinkage drying involves adhesion between the surfaces of the CNF film and filter paper rather than traditional pressure-based methods, to achieve restrained drying. Whatman® filter papers, which are non-shrinkable when dried but possess an affinity to water, were used to interact with wet CNF films. By cold pressing the wet CNF film with the filter paper, the adhesion between the two layers restricted the in-plane movement of the film without the need for additional pressure. Upon removal of the filter paper, no significant shrinkage in the diameter of the film was observed. In contrast, unrestrained drying involved placing the film directly on a metal plate surface with a spacer, which allowed air to flow through and induce radial shrinkage. Vertical shrinkage was achieved by applying pressure to both restrained and unrestrained films after drying. Refer to Fig. 3 for a visual representation of the drying methods used in this study and the shrinkage type caused by them.

Upon analysis, it was found that the average linear reduction in diameter after XY shrinkage of the films was approximately 10% compared to the initial diameter of 11 cm. Conversely, the Z_Z shrinkage did not result in any changes in the diameter. The films that experienced Z_Z shrinkage had an average thickness of 50 ± 10 µm, while the films that underwent XY_Z shrinkage had an average thickness of 60 ± 10 µm.

This result indicates that the drying process for Z_Z shrinkage led to a denser and more compacted film. Ultimately, the average density values of the films for Z_Z and XY_Z shrinkage were determined to be 0.86 g/cm^3 and 0.81 g/cm^3, respectively.

Tensile properties

The tensile strength and tensile modulus (E) were normalized by dividing them by the density of the

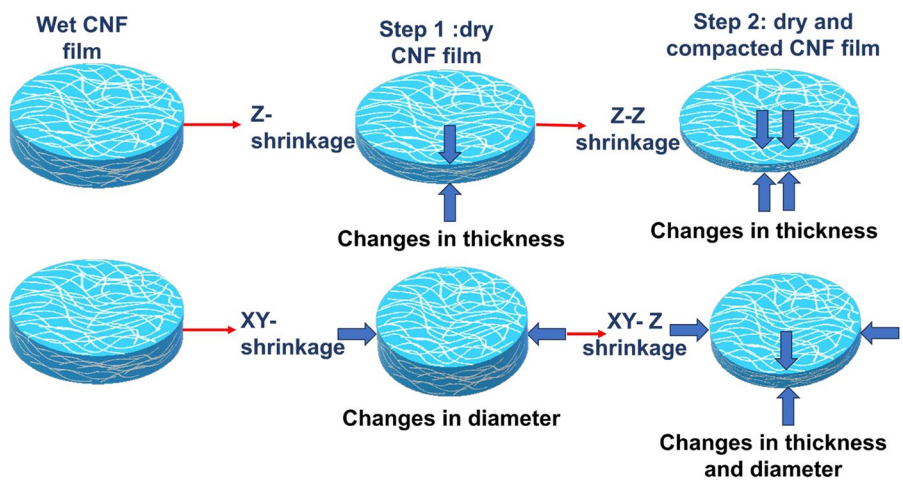

Fig. 3 The process of producing Z_Z and XY_Z shrinkage drying film

specimens as density data significantly varied among the films depending on the wire speeds and solid content of the CNF suspension. To compare the tensile properties of the ADSF films, they were evaluated against vacuum-filtered films made from a 0.3 wt.% solid content to a basis weight of 60 g/m^2. Due to the random orientation of the fibers in the film, the tensile properties were measured in one direction only.

Table S1 and Table S2 present the tensile properties of ADSF films that underwent Z_Z shrinkage drying in the machine direction and cross direction. The control vacuum-filtered samples displayed a specific strength of 41.8 ± 0.5 (MPa/(g/cm^3)), tensile strain of 5.3 ± 2.6%, and specific modulus of 3151.5 ± 783 (MPa/(g/cm^3)).

Films prepared at a speed of 1100 m/min and solids content of 0.3 wt.% exhibited the highest specific strength value of 94.3 ± 8.5 (MPa/(g/cm^3)) when tested in the machine direction, while experiencing a 10% reduction in strength in the cross direction. On the other hand, the film prepared at a speed of 1200 m/min and the same solid content had the lowest specific strength value of 54.1 ± 11(MPa/(g/cm^3)) when tested in the machine direction which decreased by 3.1% in the cross direction. This can be attributed to the instability of the forming machine at 1200 m/min leading to possible non-uniformity of the sheet formation. The statistical analysis revealed that the difference between the highest and lowest specific strength values was significant at 95% confidence level.

The highest tensile strain value observed was 1.96 ± 0.12% for the films made at 1100 m/min, 0.3 wt.% in the parallel to the machine direction which reduced to 1.71 ± 0.14% in the cross direction. On the contrary, the lowest tensile strain value found for the conditions 900 m/min and 0.3 wt. % solid content was 1.19 ± 0.08% in the machine direction which decreased to 1.01 ± 0.26% in the cross direction. However, there was no significant difference between the highest and lowest tensile strain values for Z_Z shrinkage drying method.

In the machine direction, a wire speed of 1200 m/min and solid content of 0.2 wt.% brought about the highest specific E value of 8136.5 ± 883 (MPa/(g/cm^3)), while decreasing by 18% in the cross direction. Alternatively, the ADSF film with a wire speed of 900 m/min and solid content of 0.2 wt.% had the lowest specific E value of 6742 ± 942 (MPa/(g/cm^3)) in the machine direction, which reduced by 11% in the cross direction. However, the difference between the highest and lowest specific E values was not statistically significant.

In Tables S3 and S4, the tensile properties of the ADSF films of the XY_Z shrinkage drying method for both the machine and cross directions are presented. The control sample dried using XY_Z shrinkage method showed a specific tensile strength value of 40.3 ± 12 (MPa/(g/cm^3)), a flexural strain of 6.4 ± 2.6%, and a specific E value of 2752.5 ± 647 (MPa/(g/cm^3)).

For XY_Z shrinkage drying film, films prepared at 1100 m/min wire speed and 0.1 wt.% solids content demonstrated the highest specific strength value of 61 ± 14 (MPa/(g/cm^3)) in the machine direction, but a 22% reduction in strength was observed in the cross direction. Conversely, the ADSF film with 900 m/min and 0.3 wt.% solid content had the lowest specific strength value of 43.4 ± 8 (MPa/(g/cm^3)) in the parallel direction and an 8% reduction in strength in the perpendicular direction of the machine direction. However, the difference between the highest and lowest specific strength values was not statistically significant.

Among the films dried using XY_Z shrinkage method, those made at 900 m/min, 0.1 wt.% solid content yielded the highest tensile strain value 7.0 ± 2.3% in the machine direction which was smaller than that in the cross direction (4.3 ± 1.5%). Conversely, the lowest tensile strain value in the machine direction (2.7 ± 0.94%) was found for the films made at 1100 m/min, 0.3 wt.% solid content which did not show much decrease in the cross direction. The highest and lowest tensile strain values for XY_Z shrinkage drying were found statistically different depending on the wire speeds and solid content variation.

The conditions with 1100 m/min wire speed and 0.3 wt.% solid content resulted in the highest specific modulus values (5617.7 ± 2081 (MPa/(g/cm^3))) in the machine direction for XY_Z shrinkage. However, there was a 20% decrease of specific modulus in the cross direction. On the other hand, the film with 1200 m/min wire speed and 0.2 wt.% solid content had the lowest specific modulus value of 2960.2 ± 326 (MPa/(g/cm^3)) in the machine direction. This value increased by 37% in the perpendicular direction of the machine direction. The difference between the

highest and lowest specific modulus values was significant. While the reasons for the increased specific modulus in the cross direction have not been fully explored, it is possible that the increased MOE values may be attributed to the layer-by-layer deposition of fibers in the ADSF. This could potentially lead to the misalignment of a greater number of fibers in the underlying layers when compared to the rotational direction.

In Fig. 4 the relationship between rotational speed and solid content and tensile properties is represented for the Z_Z drying method in both testing directions. The films made at the wire speed of 1100 m/min showed statistically higher tensile strength compared to those made at 900 m/min and 1200 m/min whereas they were statistically similar to the 1000 m/min films while testing in both machine and cross directions. For the tensile strain, there was no statistical difference among the films in the machine direction whereas the cross-direction data showed that the tensile strain could vary significantly depending on the wire speeds and solid content of the films.

Figure 5 displays the relationship between rotational speed, solid content, and tensile properties for the XY_Z drying method in both testing directions. The results indicate that the specific tensile strength values were significantly different from each other depending on the wire speed and solid content of the CNF suspension in both directions. The statistical analysis of the tensile strain revealed significant variations both in the machine and cross directions, which were found to be dependent on the wire speeds and solid content of the films.

It was determined that both 1000 m/min and 1100 m/min wire speeds are suitable for producing films with favorable mechanical properties, regardless

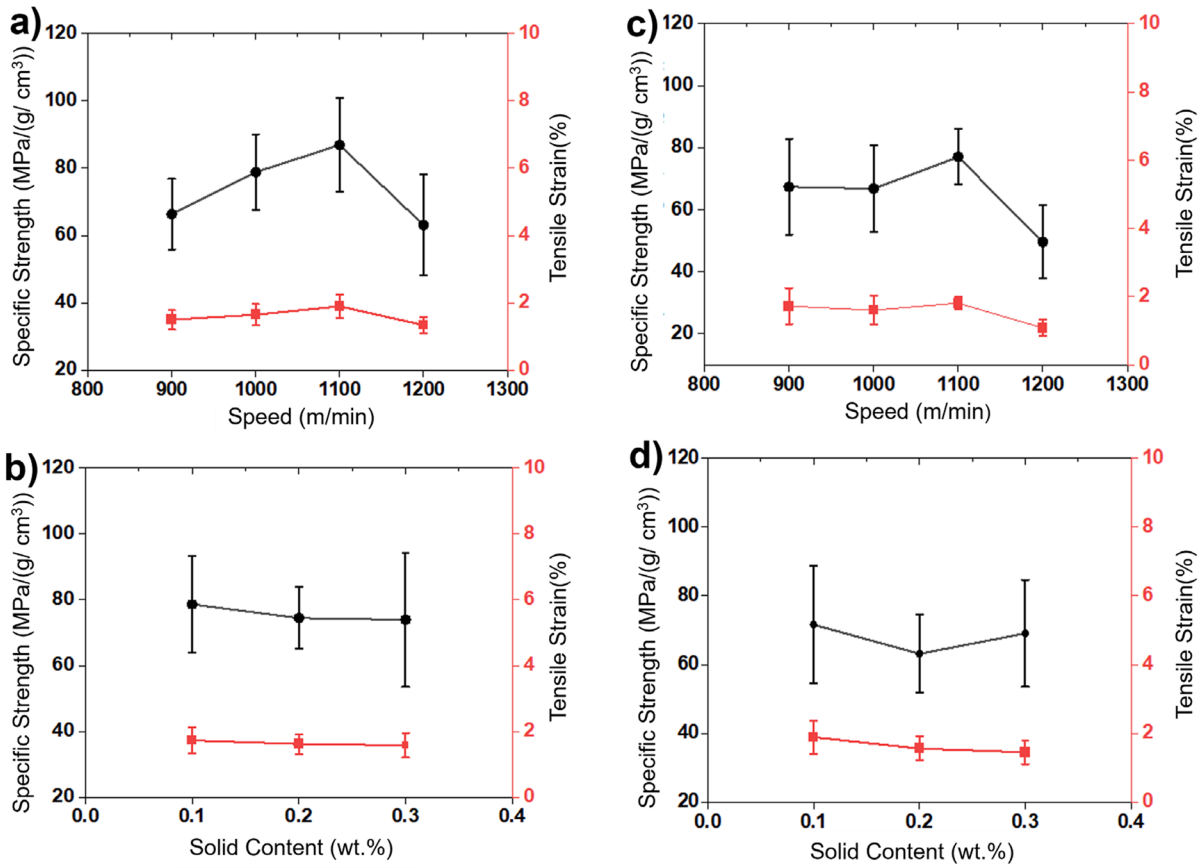

Fig. 4 Tensile properties as a function of **a** wire speed, **b** solid content in the parallel direction and tensile properties as a function of **c** wire speed and **d** solid content in the perpendicular direction of samples made using the Z_Z drying method

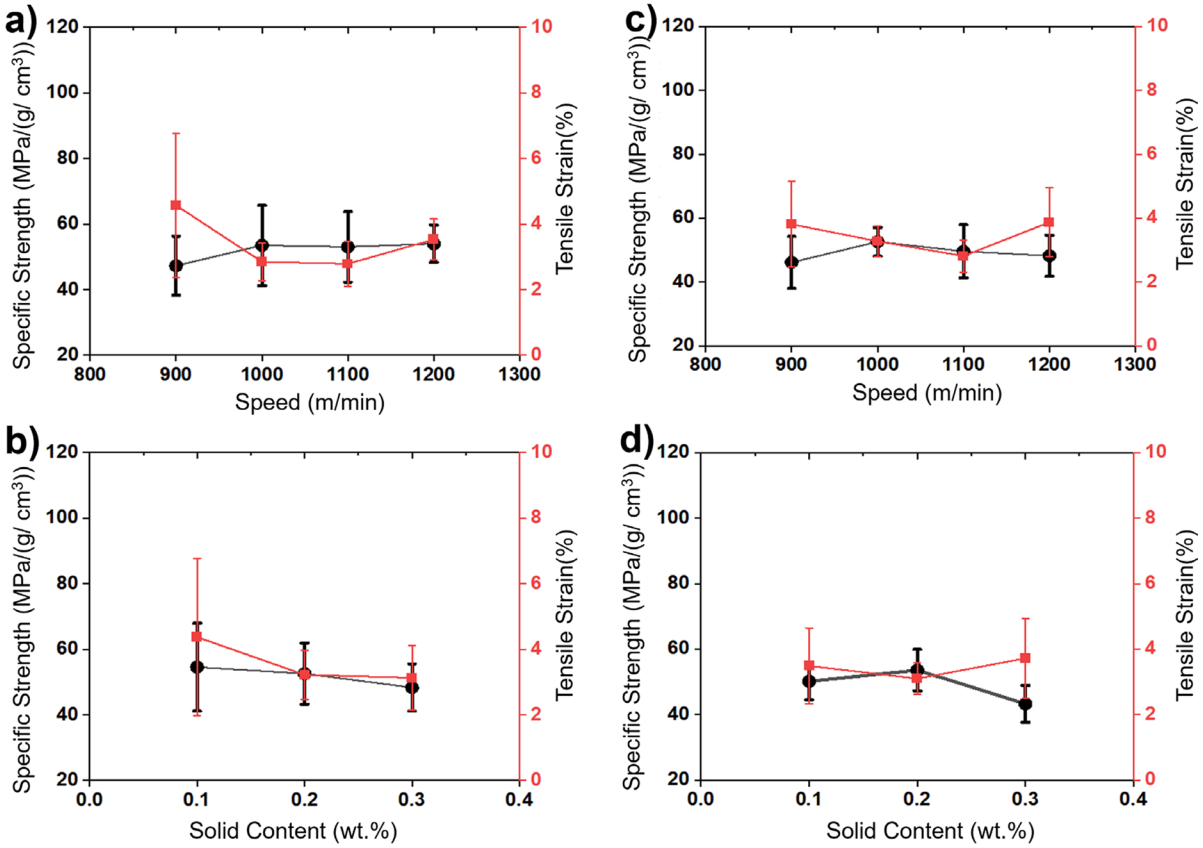

Fig. 5 Tensile properties as a function of **a** wire speed and **b** solid content in the parallel direction and tensile properties as a function of **c** wire speed, **d** solid content in the perpendicular direction in the XY_Z drying method

of the drying method. Previous research has also indicated that wire speed significantly impacted the film's alignment and mechanical properties (Zhang et al. 2014; Markatos et al. 2018). To enhance alignment and mechanical properties, wire speed optimization is necessary, taking into account the machine's capabilities since optimized wire speeds can both align fibers and hold the bulk of the fiber on the wire mesh (Gigac and Fišerová 2010). The lowest and highest wire speeds utilized in this study to develop an oriented sheet were insufficient in holding more fibers on the surface of the wire mesh and resulted in a non-uniform fiber distribution on the film surface, which may have contributed to lower mechanical properties.

According to Li et al. 2021, the alignment of fibers in a film can be determined by calculating its anisotropy ratio. This ratio corresponds to the tensile properties of the film in the machine direction versus the cross direction of ADSF, and a value higher than 1 indicates better orientation. To obtain the anisotropy ratio in this study, the specific modulus values of the machine direction were divided by the cross-direction modulus values. Results showed that the film with the maximum anisotropy ratio (1.41) was produced using Z_Z drying at a wire speed of 1000 m/min and the minimum anisotropy ratio (1.06) calculated for 900 m/min, while films dried using XY_Z method at 1100 m/min yielded the maximum anisotropy ratio of 1.38 and those made at 1200 m/min showed the minimum anisotropy ratio of 0.82.

In Fig. 6, a comparison is presented regarding the tensile properties based on the drying method. It was found that for Z_Z shrinkage drying, the machine direction specific tensile strength of 1000 m/min and 1100 m/min films increased by 47% and 63%, respectively, compared to the XY_Z shrinkage dried films.

The specific strength of the Z_Z shrinkage dried films at 1000 m/min and 1100 m/min wire speed

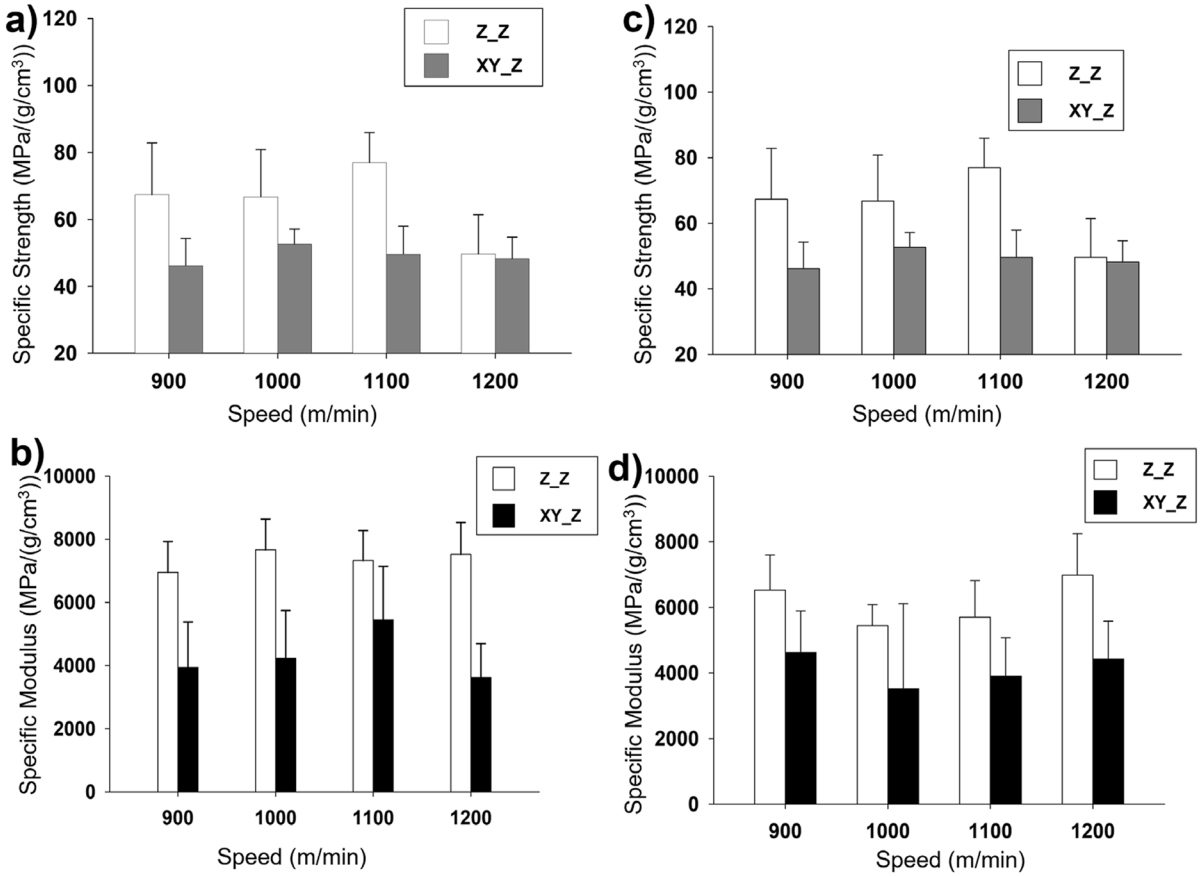

Fig. 6 Comparison of tensile properties between the drying methods **a-b** in the parallel direction and **c-d** in the perpendicular direction depending on the wire speed

was raised by 46% and 57%, respectively, compared to the XY_Z drying method when evaluated in the cross direction. Additionally, the films showed a similar trend of increased mechanical properties for Z_Z drying in both the parallel and perpendicular direction of machine motion when evaluating the specific modulus values. During unrestrained drying while the film shrank radially, there is a possibility that the longer and flexible CNF fibers could bend or form coils in the films. When tensile stress is applied, the fibrils within the film may undergo uncoiling or straightening. This increases the tensile strain of the film while reducing stiffness (Fig. 7) (Ritchie 2011; Kouko and Retulainen 2018; Ghasemi et al. 2020). This can explain the increase of the tensile strain for XY_Z dried films while reducing the tensile strength compared to Z_Z dried films.

Oxygen barrier properties

Food packaging plays a crucial role in maintaining the quality, freshness, and marketability of food products. An essential factor in food packaging is the oxygen barrier property, which prevents oxygen from passing through the packaging material and causing food spoilage and microbial activity.

In Fig. 8, the oxygen transmission rate (OTR) and oxygen permeability (OP) of ADSF films dried using the Z_Z shrinkage method at 80% RH are displayed. The highest OTR value (17.4 ± 5.1 (cc/m^2.day)) was observed for the conditions of 900 m/min wire speed and 0.1% solid content of CNF suspension while the lowest OTR value (6 ± 0.5 (cc/m^2.day)) was observed for the conditions of 1100 m/min wire speed and 0.1% solid content of CNF suspension. Additionally, the vacuum filtered films exhibited a slightly lower OTR

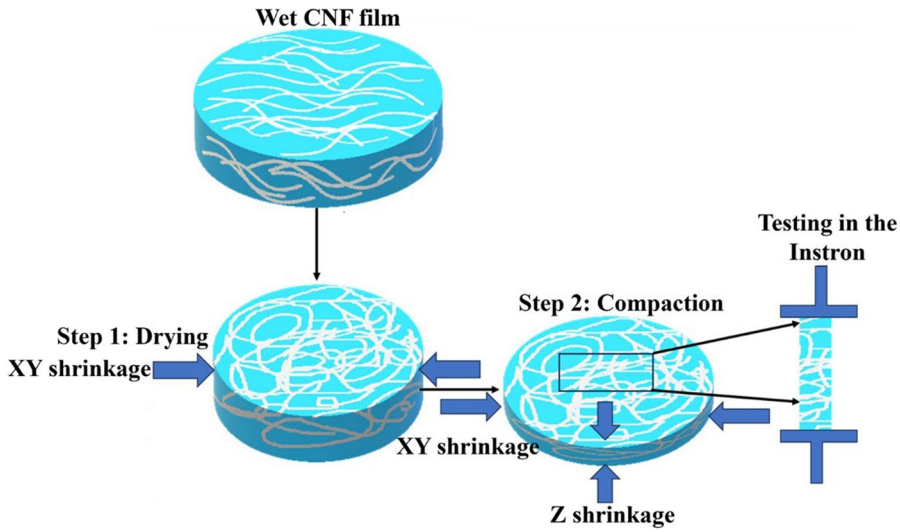

Fig. 7 Schematic diagram of the coiling effect of the fibrils due to unrestrained shrinkage

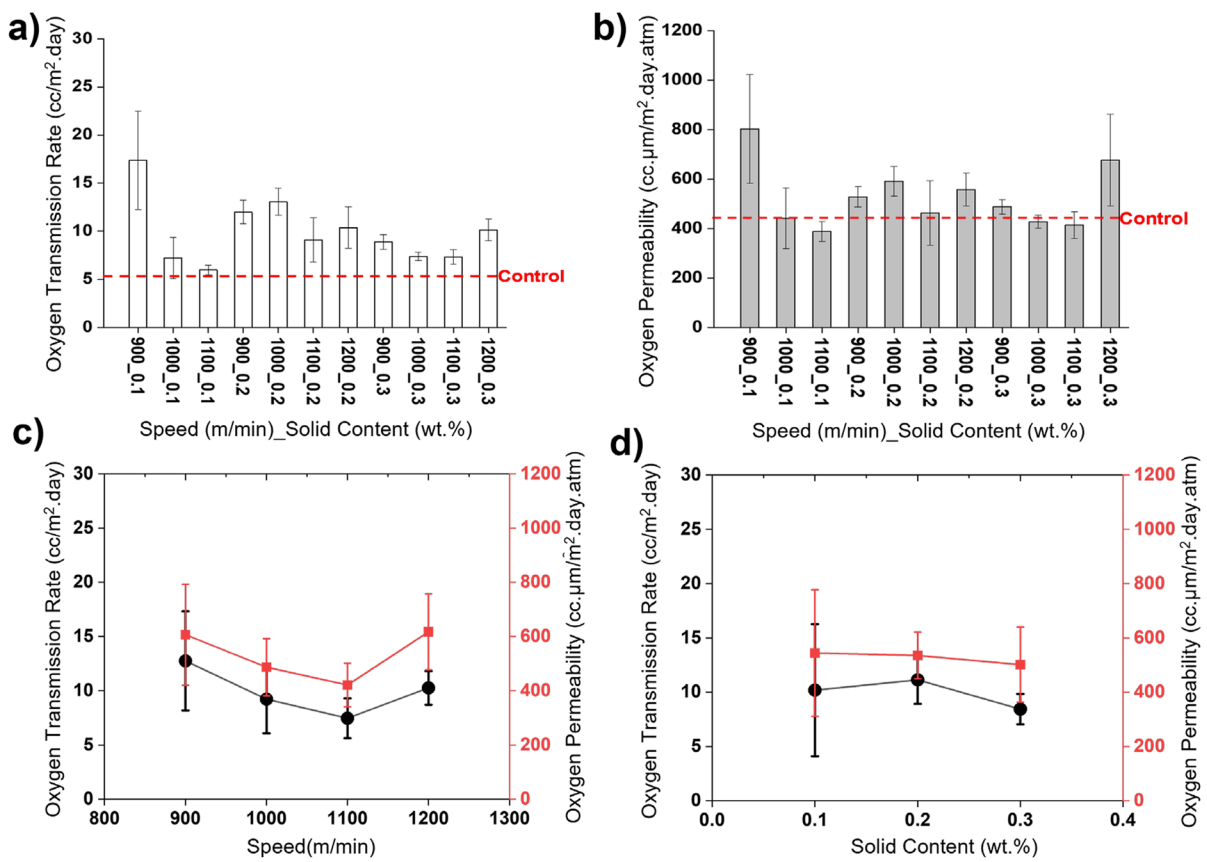

Fig. 8 **a** Oxygen transmission rate, **b** Oxygen permeability of the ADSF film and the relationship of oxygen barrier properties with **c** wire speed, and **d** CNF solid content for the Z_Z drying method

value (5.4 ± 0.1 (cc/m^2.day)) than the ADSF film prepared at 1100 m/min wire speed. One possible reason for obtaining lower OTR values for the control sample is that in the vacuum-filtration process, no agitation or motion was involved which produced very low shear forces during film formation which may have contributed to more uniform and denser films leading to lower OTR value (Osterberg et al. 2013).

According to Wang et al. (2018a, b), the thickness and relative humidity of a film greatly impact the rate at which oxygen can pass through it. To accurately determine a film's oxygen permeability, OTR values must first be normalized to account for thickness variations. The ADSF films with 0.1% solid content and a wire speed of 1100 m/min demonstrated the lowest OP value of 387.7 ± 40 (cc.µm/m^2.day.atm), while the CNF films with 0.1% solid content and a wire speed of 900 m/min had the highest OP value of 803 ± 220 (cc.µm/m^2.day.atm). It is observable that the OP values of the 1100 m/min wire speed and 0.1% solid content ADSF films showed an 11.4% reduction compared to the vacuum-filtered samples.

For Z–Z shrinkage drying, based on wire speed, various differences were observed in ADSF films for oxygen barrier properties. Oxygen barrier properties were lower in the 900 m/min films, whereas the 1100 m/min films presented higher oxygen barrier properties. Moreover, the 1100 m/min films were found to be more oriented than the 900 m/min films, according to anisotropy ratio evaluation. Through hot press compaction and a more anisotropic fiber alignment, free volume was reduced by increasing packing density, leading to a more tortuous path for oxygen to pass through the film.

The results presented in Fig. 9a, b illustrate the oxygen barrier properties of the XY_Z shrinkage films. According to the mechanical properties analysis of XY_Z shrinkage films, it was calculated that the 900 m/min films may have a lower anisotropy ratio, suggesting a potential for less orientation in the film. In contrast, the 1100 m/min films demonstrated a higher anisotropy ratio, indicating a possibility of higher films' orientation in the XY_Z shrinkage drying process. To investigate the correlation between CNF alignment in the film and barrier properties, the oxygen barrier properties of the 900 m/min and 1100 m/min films were examined. Furthermore, the 900 m/min, 0.1 wt.% and 1100 m/min, 0.1 wt.% films were selected for oxygen barrier properties testing of the XY_Z shrinkage method due to their higher and lower oxygen permeability values, respectively, for Z_Z shrinkage drying.

It was observed that the OTR of the films made at 900 m/min and 0.1 wt.% was 9.5% higher value than that of 1100 m/min. Additionally, the oxygen permeability values determined by normalizing the OTR values revealed that the 900 m/min /0.1 wt.% films had a 40.5% higher permeability value than the 1100 m/min/0.1 wt.% film, which is consistent with the Z_Z shrinkage method findings. The vacuum-filtered control sample also demonstrated 4.3% lower oxygen permeability values than the 1100 m/min film, similar to the Z_Z shrinkage drying method. However, the difference between the oxygen permeability value of control sample and 1100 m/min were not significantly different.

Figure 9c–d indicates the comparison between the Z_Z shrinkage drying method and XY_Z shrinkage drying method oxygen barrier properties for 900 m/min, 0.1 wt.% and 1100 m/min, 0.1 wt.% films. For the films made at 900 m/min, 0.1 wt.%, it was found that the XY_Z shrinkage drying method resulted in the OTR and OP values that were 52% and 29% lower (improved barrier properties) than the corresponding films dried using the Z_Z shrinkage drying method, respectively. CNF films can be significantly self-oriented when subjected to an un-restrained drying method (Ghasemi et al. 2020) which could contribute to the improvements in the oxygen barrier properties for XY_Z shrinkage drying method.

At a speed of 1100 m/min and a concentration of 0.1 wt.%, the XY_Z shrinkage drying method was found to result in lower OP values by 12%, compared to the Z_Z shrinkage drying method. Though there was so statistical difference found for the OP values of two drying methods while comparing within a specific wire speed. The anisotropy ratio of the film made at 1100 m/min was found to be 1.4 for both drying methods, which suggests that they do not differ in orientation in terms of mechanical properties. Therefore, it is possible that the variance in oxygen barrier characteristics between Z_Z and XY_Z shrinkage film of 1100 m/min wire speed can be attributed to the shrinkage drying process used for each. From the density calculation, it was found that Z_Z experienced a significant increase in density, leading to a narrower gas passage pathway in the denser films.

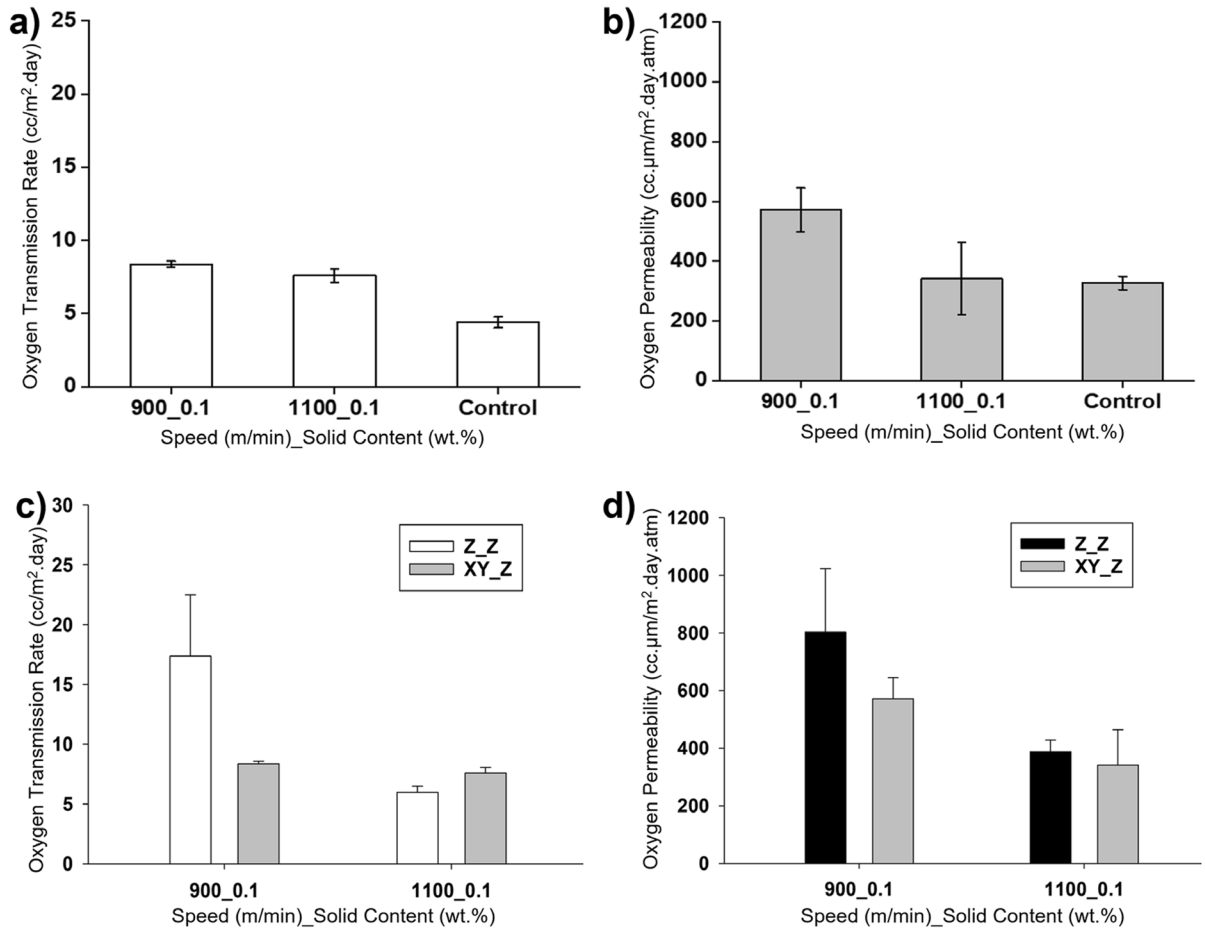

Fig. 9 **a** Oxygen transmission rate, **b** Oxygen permeability of the ADSF film for XY_Z drying method and the comparison between Z_Z shrinkage drying method and XY_Z shrinkage drying method depending on **c** Oxygen transmission rate, **d** Oxygen permeability of the ADSF film

As a result, oxygen gas permeance through the films could be reduced.

To gain a better understanding of the correlation between films' orientation and their barrier properties, we further quantified the degree of orientation in the subsequent section. This can provide greater clarity on the connection between films orientation and their barrier properties.

Polarized light microscopy

Based on the findings of mechanical and barrier properties, it was discovered that the film made with a wire speed of 900 m/min and 0.1 wt.% CNF solid content could potentially have the least CNF orientation, while the film made with a wire speed of 1100 m/min and 0.1 wt.% CNF solid content of could possibly have higher CNF orientation.

Figure 10 reveals the classified maps of BOI values for wire speeds of 900 m/min and 1100 m/min, with a solid content of 0.1 wt. %. These maps indicate the range of BOI values and the level of fiber alignment in the film for both Z_Z and XY_Z shrinkage drying methods. The Z_Z shrinkage drying method revealed a median BOI value of + 0.05 for ADSF films with 0.1% solid content and a wire speed of 1100 m/min, whereas the median BOI value for the same CNF solids content ADSF film made with a wire speed of 900 m/min was found to be + 0.03. The median BOI value for the XY_Z shrinkage drying method was determined to be + 0.02 for ADSF films with 0.1% solid content and a wire speed of 1100 m/

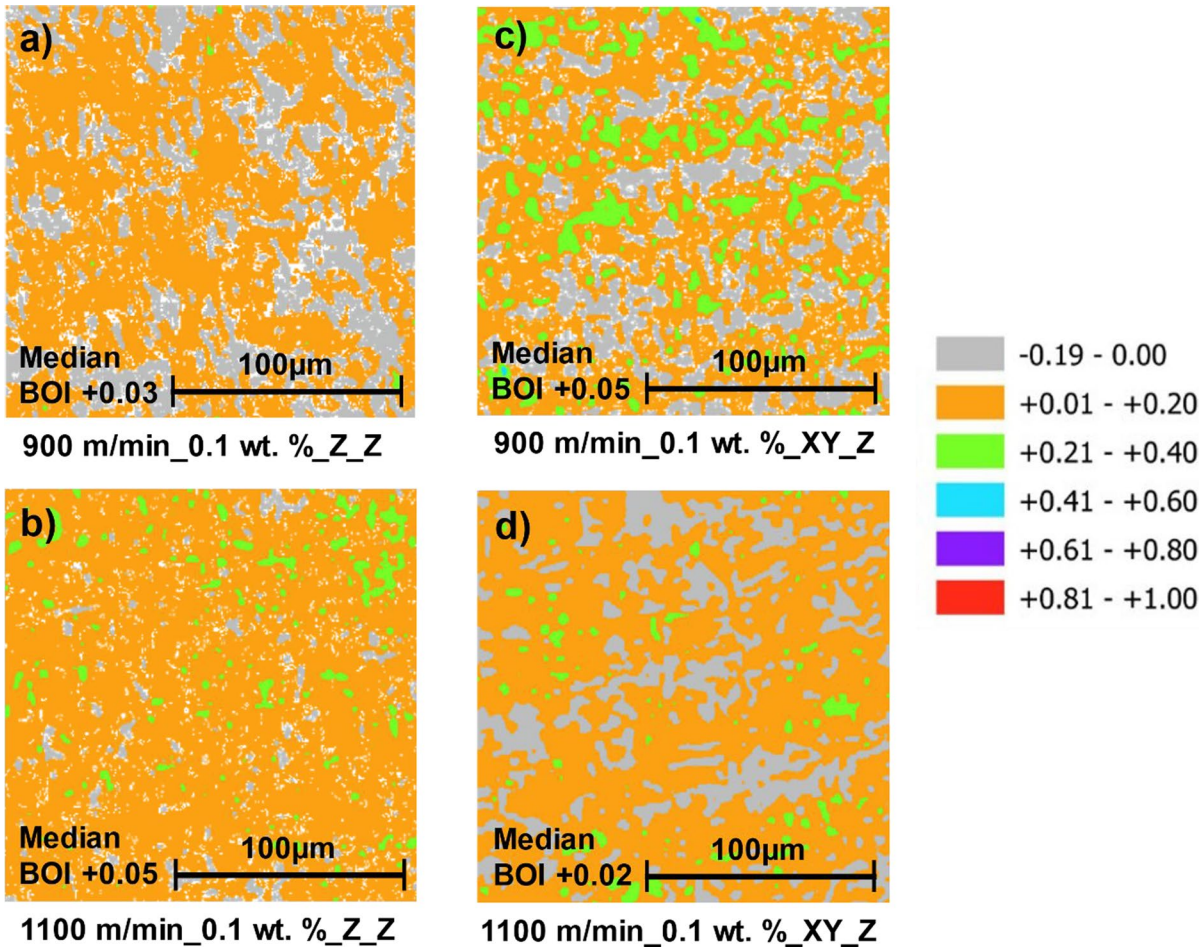

Fig. 10 The classified map of the BOI index for Z_Z and XY_Z shrinkage drying

min. However, at a wire speed of 900 m/min and the same solids content, the median BOI value increased to + 0.05 Overall, the changes in median BOI values do not seem to be conclusive, perhaps because of the low level of overall orientation of CNFs in the films.

Comparing the frequency of pixels with higher BOI values in Fig. 10, however, some general trends can be observed. Firstly, comparing Fig. 10a with Fig. 10b indicates that for Z–Z films, the increased wire speed led to better orientation in the direction of wire rotation. This is evident with the relatively lower number of gray pixels (negative values) in Fig. 10b compared to Fig. 10a. However, an opposite trend was observed for the XY_Z films where an increase in wire speed led to lower orientation in the machine direction.

The CNFs are able to instigate a significant amount of autogenous orientation in the films when dried un-restrained in all directions (Ghasemi et al. 2020). From the mechanical properties, it appears that the 900 m/min, 0.1 wt.% films had a lower anisotropy ratio, which suggests that there was a low level of orientation. In the Z–Z films that are dried under restraint, it can be expected that the original orientation developed during film formation can be largely retained. However, the unrestrained XY_Z drying may be able to impart additional orientation upon drying. This finding is consistent with a previous study that employed the unrestrained drying method (Ghasemi et al. 2020). It is worth noting that the anisotropy ratio of the 1100 m/min, 0.1 wt.% films indicated better CNF orientation in the films.

Various factors may result in differences between BOI and the anisotropic ratio, including the variation in fiber orientation within the film layers during formation and the limited range of examination with polarized light microscopy. In the course of ADSF's film production, it was noted that the process involved transverse movement of the nozzle to spray the fiber suspension and form a fiber mat of the required thickness, which entailed layer-by-layer fiber deposition. This technique could potentially result in fiber misalignment within the film analyzed by polarized light microscopy.

Wide-angle X-ray scattering property

Wide angle X-ray scattering is a widely employed technique utilized for the assessment of fibril orientation in CNF films. The diffraction pattern obtained through this approach effectively reveals the crystallographic lattice planes present in the sample, allowing for a comprehensive evaluation of their properties (Li et al. 2021).

Figure 11 represents the X-ray diffractograms in the parallel and perpendicular direction to the wire rotation of 900 m/min and 1100 m/min of restrained and un-restrained dried films of 0.1 wt.%. According to (Wang et al. 2018b), an increased luminosity in the arcs in any direction would indicate an augmentation in alignment within the tested portion of the film in that direction. Figure 11 exhibits no changes in the intensity between the vertical and horizontal directions of the films. The observed outcome could potentially be attributed to either the inadequate alignment of fibrils in the film portion during its production, which was used for wide angle X-ray scattering analysis, or the effect of self-orientation caused by unrestricted drying. Given that mechanical property data confirmed significant orientation, the failure of wide-angle X-ray diffractograms to confirm the same may be attributed to localized orientations captured in wide-angle X-ray diffractograms measurements or the fact that the system used a line collimation setup instead of point collimation. These findings hold significant implications for further research in this area, particularly in terms of optimizing the production and

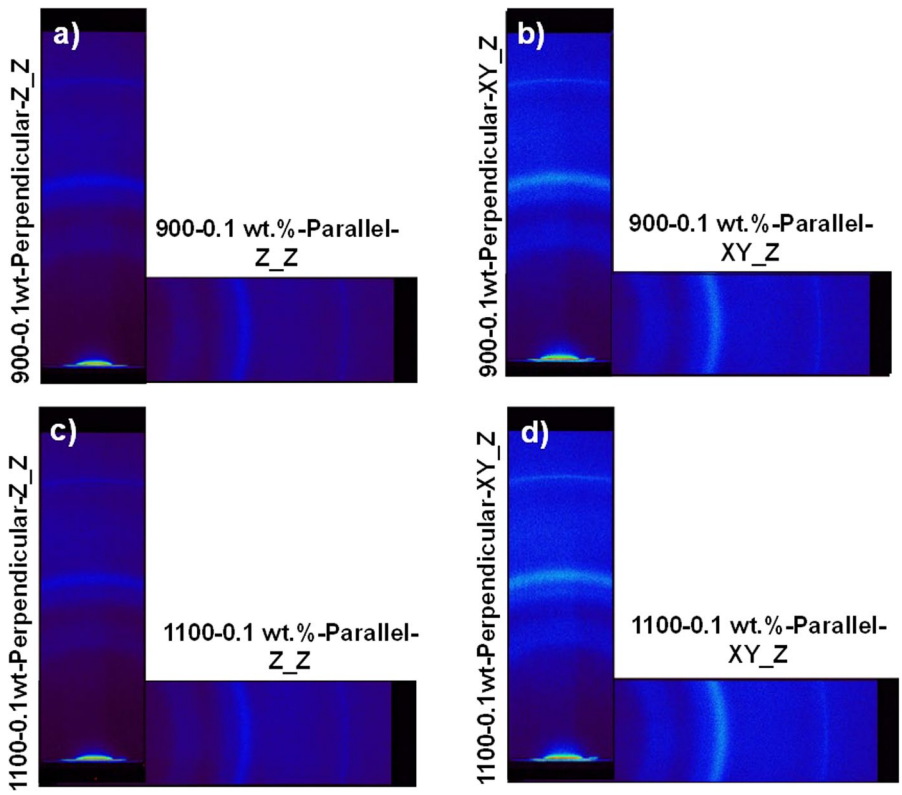

Fig. 11 Wide angle X-ray scattering diffractograms of the ADSF films in the parallel and perpendicular direction to the wire rotation for restrained (**a** and **c**) and un-restrained (**b** and **d**) films

drying processes to ensure greater alignment and orientation of fibrils for improved outcomes.

Conclusions

In this study, cellulose nanofibril (CNF) films were prepared in a two-step process involving a formation process followed by different drying techniques: We used an auto-dynamic sheet former (ADSF) to form the wet mats and either an induced-shrinkage drying technique or a restrained (no in-plane shrinkage) technique. The XY_Z films exhibited a 10% reduction in diameter compared to their initial wet sizes, while the Z_Z film showed no significant change in diameter. Additionally, the density of the Z_Z shrinkage films was increased by 6.2% in comparison to the XY_Z shrinkage films. The optimized wire speeds and solid content in the ADSF process resulted in higher mechanical strength and tensile properties for the restrained Z_Z drying, whereas the non-restrained XY_Z drying method exhibited an increase in the tensile strain properties of the films. The anisotropy ratio indicated that it is possible to achieve relatively oriented native CNF films by optimizing the wire speed and solid content of the suspension.

The anisotropy ratio calculated for the film produced at the optimized wire speed correlated well with a lower oxygen permeability value. This finding suggests that a relatively high degree of orientation in the CNFs could potentially enhance the barrier properties of the film. Considering both drying techniques, 1100 m/min films were able to resist more oxygen than 900 m/min films. To gain a more comprehensive understanding of the degree of orientation within the film, polarized light microscopy and wide-angle X-ray scattering were employed. However, polarized light microscopy and wide-angle X-ray scattering images were highly localized, providing insights into only a small area, making it challenging to assess the orientation of fibers across the entire film and relating those to the barrier or mechanical properties. Nevertheless, the anisotropy ratio obtained from mechanical testing and differences in oxygen barrier properties offered substantial indicators of the film's internal orientation.

Moving forward, a few limitations of this study can be noted and considered for future research. First, the auto dynamic sheet former used in this study had limitations in the range of wire speed as higher speeds than those used in this study would lead to machine instability and termination of sheet forming. Having a wider range of wire speeds could potentially lead to a better distinction of alignment among treatments. Also, we evaluated the orientation of the films using polarized light microscopy (PLM) and wide-angle X-ray scattering (WAXS). However, these methods seemed to be limited to specific instances, as only a small area of the film could be assessed which did not provide a comprehensive indication of the overall alignment of the film, likely due to averaging of film's response to these techniques caused by their multilayer structure. If possible, thinner CNF films could be produced, which would make it easier to evaluate nanofibril orientation. The wide-angle X-ray scattering system utilized in this investigation was found to be incapable of generating intensity profiles from the data. Wide-angle X-ray scattering intensity profiles can only be generated from point collimation.

Overall, this research reveals the optimized relationship between the wire speed in ADSF and the solid content of native CNF, leading to the production of relatively oriented CNF sheets. It also explains how the induced-shrinkage drying method and fiber orientation collectively impact the mechanical and barrier properties of CNF films, making them a promising choice for food packaging materials such as packages of fresh ground coffee or sliced apples wrapped in CNF films. Above all, this research contributes to our efforts to combat plastic pollution and protect the environment.

Author contributions The study's conception and design resulted from a collaborative effort among all authors. Mehdi Tajvidi and Islam Hafez oversaw material preparation, data collection, and analysis. The initial draft of the manuscript was composed by Nabanita Das, with all authors contributing feedback on earlier iterations. All authors thoroughly reviewed and endorsed the final version of the manuscript.

Funding This project received support from the Maine Agricultural and Forest Experiment Station and the Paper Surface Science Program at the University of Maine.

Data availability No datasets were generated or analysed during the current study.

Declarations

Competing interests The authors declare no competing interests.

Ethical approval Not applicable.

References

Amini E, Hafez I, Tajvidi M, Bousfield DW (2020) Cellulose and lignocellulose nanofibril suspensions and films: a comparison. Carbohydr Polym 250:117011. https://doi.org/10.1016/j.carbpol.2020.117011

Aulin C, Gällstedt M, Lindström T (2010) Oxygen and oil barrier properties of microfibrillated cellulose films and coatings. Cellulose 17:559–574. https://doi.org/10.1007/s10570-009-9393-y

Bharadwaj RK (2002) Effect of H2O on the diffusion of N2 in PMMA: a molecular dynamics simulation study. Macromolecules 35:5334–5336. https://doi.org/10.1021/ma020342k

Chowdhury RA, Nuruddin M, Clarkson C et al (2018) Cellulose nanocrystal (CNC) coatings with controlled anisotropy as high-performance gas barrier films. ACS Appl Mater Interfaces 11:1376–1383. https://doi.org/10.1021/acsami.8b16897

D3985-05 A (2010) Standard test method for oxygen gas transmission rate through plastic film and sheeting using a coulometric sensor. ASTM International, Philadelphia. https://doi.org/10.1520/D3985-05R10E01

Dlubek G, Redmann F, Krause-Rehberg R (2002) Humidity-induced plasticization and antiplasticization of polyamide 6: a positron lifetime study of the local free volume. J Appl Polym Sci 84:244–255. https://doi.org/10.1002/app.10319

Dufresne A (2017) Nanocellulose: from nature to high performance tailored materials. Walter de Gruyter GmbH & Co KG, Berlin. https://doi.org/10.1515/9783110480412-001

Fujisawa S, Togawa E, Hayashi N (2016) Orientation control of cellulose nanofibrils in all-cellulose composites and mechanical properties of the films. J Wood Sci 62:174–180. https://doi.org/10.1007/s10086-015-1533-4

Fukuya MN, Senoo K, Kotera M et al (2014) Enhanced oxygen barrier property of poly (ethylene oxide) films crystallite-oriented by adding cellulose single nanofibers. Polymer 55:5843–5846. https://doi.org/10.1016/j.polymer.2014.09.003

Geueke B, Phelps DW, Parkinson LV, Muncke J (2023) Hazardous chemicals in recycled and reusable plastic food packaging. Camb Prisms Plast 1:e7. https://doi.org/10.1017/plc.2023.7

Ghasemi S, Rahimzadeh-Bajgiran P, Tajvidi M, Shaler SM (2020) Birefringence-based orientation mapping of cellulose nanofibrils in thin films. Cellulose 27:677–692. https://doi.org/10.1007/s10570-019-02821-2

Ghasemi S, Tajvidi M, Bousfield DW et al (2017) Dry-spun neat cellulose nanofibril filaments: influence of drying temperature and nanofibril structure on filament properties. Polymers 9:392. https://doi.org/10.3390/polym9090392

Gigac J, Fišerová M (2010) Effect of velocity gradient on papermaking properties. Cellul Chem Technol 44:389

Gindl W, Keckes J (2007) Drawing of self-reinforced cellulose films. J Appl Polym Sci 103:2703–2708. https://doi.org/10.1002/app.25434

Gindl-Altmutter W, Veigel S, Obersriebnig M et al (2012) High-modulus oriented cellulose nanopaper. In: Functional materials from renewable sources. ACS Publications, pp 3–16. https://doi.org/10.1021/bk-2012-1107.ch001

Hasan I, Wang J, Tajvidi M (2021) Tuning physical, mechanical and barrier properties of cellulose nanofibril films through film drying techniques coupled with thermal compression. Cellulose 28:11345–11366. https://doi.org/10.1007/s10570-021-04269-9

Johnson D, Papadis M, Bilodeau M et al (2016) Effects of cellulosic nanofibrils on papermaking properties of fine papers. TAPPI J 15:395–402. https://doi.org/10.32964/TJ15.6.395

Kouko J, Retulainen E (2018) The relationship between shrinkage and elongation of bleached softwood kraft pulp sheets. Nord Pulp Pap Res J 33:522–533. https://doi.org/10.1515/npprj-2018-3057

Li K, Clarkson CM, Wang L et al (2021) Alignment of cellulose nanofibers: harnessing nanoscale properties to macroscale benefits. ACS Nano 15:3646–3673. https://doi.org/10.1021/acsnano.0c07613

Markatos DN, Sarakinis A, Mavrilas D (2018) Tuning fiber alignment to achieve mechanical anisotropy on polymeric electrospun scaffolds for cardiovascular tissue engineering. J Mater Sci Eng 7:466. https://doi.org/10.4172/2169-0022.1000466

Moon RJ, Martini A, Nairn J et al (2011) Cellulose nanomaterials review: structure, properties and nanocomposites. Chem Soc Rev 40:3941–3994. https://doi.org/10.1039/C0CS00108B

Mörseburg K, Chinga-Carrasco G (2009) Assessing the combined benefits of clay and nanofibrillated cellulose in layered TMP-based sheets. Cellulose 16:795–806. https://doi.org/10.1007/s10570-009-9290-4

Muramatsu M, Okura M, Kuboyama K et al (2003) Oxygen permeability and free volume hole size in ethylene–vinyl alcohol copolymer film: temperature and humidity dependence. Radiat Phys Chem 68:561–564. https://doi.org/10.1016/S0969-806X(03)00231-7

Nair SS, Zhu JY, Deng Y, Ragauskas AJ (2014) High performance green barriers based on nanocellulose. Sustain Chem Process 2:1–7. https://doi.org/10.1186/s40508-014-0023-0

Nazari B, Kumar V, Bousfield DW, Toivakka M (2016) Rheology of cellulose nanofibers suspensions: boundary driven flow. J Rheol 60:1151–1159. https://doi.org/10.1122/1.4960336

Ncube LK, Ude AU, Ogunmuyiwa EN et al (2020) Environmental impact of food packaging materials: a review of contemporary development from conventional plastics to polylactic acid based materials. Materials 13:4994. https://doi.org/10.3390/ma13214994

Osterberg M, Vartiainen J, Lucenius J et al (2013) A fast method to produce strong NFC films as a platform for barrier and functional materials. ACS Appl Mater Interfaces 5:4640–4647. https://doi.org/10.1021/am401046x

Peng J, Ellingham T, Sabo R et al (2015) Oriented polyvinyl alcohol films using short cellulose nanofibrils as a reinforcement. J Appl Polym Sci. https://doi.org/10.1002/app.42283

Petroudy SRD, Garmaroody ER, Rudi H (2017) Oriented cellulose nanopaper (OCNP) based on bagasse cellulose nanofibrils. Carbohydr Polym 157:1883–1891. https://doi.org/10.1016/j.carbpol.2016.11.074

Ritchie RO (2011) The conflicts between strength and toughness. Nat Mater 10:817–822. https://doi.org/10.1038/nmat3115

Sehaqui H, Ezekiel Mushi N, Morimune S et al (2012) Cellulose nanofiber orientation in nanopaper and nanocomposites by cold drawing. ACS Appl Mater Interfaces 4:1043–1049. https://doi.org/10.1021/am2016766

Sunny T, Pickering KL, McDonald-Wharry J (2021) Improving the alignment of dynamic sheet-formed mats by changing nozzle geometry and their reinforcement of polypropylene matrix composites. J Compos Sci 5:226. https://doi.org/10.3390/jcs5090226

Syverud K, Stenius P (2009) Strength and permeability of MFC films. Cellulose 16:75–85. https://doi.org/10.1007/s10570-008-9244-2

Tajvidi M, Gardner DJ, Bousfield DW (2016) Cellulose nanomaterials as binders: laminate and particulate systems. J Renew Mater 4:365. https://doi.org/10.7569/JRM.2016.634103

Tucki K, Orynycz O, Wasiak A et al (2022) Potential routes to the sustainability of the food packaging industry. Sustainability 14:3924. https://doi.org/10.3390/su14073924

Wang J, Gardner DJ, Stark NM et al (2018a) Moisture and oxygen barrier properties of cellulose nanomaterial-based films. ACS Sustain Chem Eng 6:49–70. https://doi.org/10.1021/acssuschemeng.7b03523

Wang L, Chen C, Wang J et al (2020) 17 Cellulose nanofibrils versus cellulose nanocrystals: comparison of performance in flexible multilayer films for packaging applications. Food Packag Shelf Life 23:100464. https://doi.org/10.1016/j.fpsl.2020.100464

Wang S, Li T, Chen C et al (2018b) Transparent, anisotropic biofilm with aligned bacterial cellulose nanofibers. Adv Funct Mater 28:1707491. https://doi.org/10.1002/adfm.201707491

Xu X, Liu F, Jiang L et al (2013) Cellulose nanocrystals vs. cellulose nanofibrils: a comparative study on their microstructures and effects as polymer reinforcing agents. ACS Appl Mater Interfaces 5:2999–3009. https://doi.org/10.1021/am302624t

Zabihzadeh Khajavi M, Ebrahimi A, Yousefi M et al (2020) Strategies for producing improved oxygen barrier materials appropriate for the food packaging sector. Food Eng Rev 12:346–363. https://doi.org/10.1007/s12393-020-09235-y

Zhang FD, Pei JC, Li J et al (2014) The effect of speeds of jet and wire on the physical properties of paper sheets forming in a dynamic sheet former. China Pulp Pap 33:25–30. https://doi.org/10.11980/j.issn.0254-508X.2014.06.005